SUBMITTED FOR PUBLICATION IN:
Meteoritics & Planetary Science REFEREE VERSION

June 1, 1999

Activity of the 1998 Leonid shower from video records

PETER JENNISKENS[1*]

[1]SETI Institute, NASA Ames Research Center, Mail Stop 239-4, Moffett Field, CA 94035

*Corresponding author's e-mail address: peter@max.arc.nasa.gov

Abstract. Video observations of the 1998 Leonid shower aboard two aircraft in the 1998 Leonid Multi-Instrument Aircraft Campaign and from ground locations in China are presented. 4200 video meteors are available for analysis. Observations from aircraft proved particularly effective, with four times higher rates of meteors due to low extinction and low angular velocity at the horizon. Two distinct dust components were mapped. One dominated the night of Nov. 16/17. This two-day wide broad component peaked at $\lambda o = 234.52$ at the influx of $3.3 \pm 0.4 \times 10^{-12}$ m^{-2} s^{-1} for particles of mass $< 7 \times 10^{-5}$ gram, and was rich in bright meteors with $r = N(m+1)/N(m) \sim 1.5$ ($s = 1.4$). The dominant influx occurred in the next night of Nov. 17/18, near the node of the parent comet. Rates were elevated above the broad component between $\lambda o = 235.15$ and 235.40, symmetric around the current node of the parent comet 55P/Tempel-Tuttle, peaking at $4.2 \pm 0.2 \times 10^{-12}$ m^{-2} s^{-1} at solar longitude $\lambda o = 235.32$. The magnitude distribution had a population index of $r = 1.8 \pm 0.1$ ($s = 1.7$). The flux profile of this component is asymmetric and may consist of a blended contribution from at least two different but relatively recent epochs of ejection. Similar components were seen in other years, but this time they were separated in node. No peak of faint meteors was observed (e.g. Leonid storms in the past had $r = 3.0$), with the exception of an isolated 5-minute interval at $\lambda o = 235.198$, perhaps the result of a meteoroid breakup.

INTRODUCTION

At no other time since the meteor storm of 1966 was there so much interest in the activity of the Leonid meteor shower than in the anticipation of the November 1998 return. The Earth was expected to cross relatively recent ejecta of parent comet 55P/Tempel-Tuttle, back at perihelion on February 1998, potentially raising Leonid shower rates above 1 per second (Yeomans et al. 1996, Jenniskens 1996). The encounter raised concerns about enhanced collision rates of meteoroids with satellites (Beech & Brown 1994), but also raised hopes that such recent ejecta could be studied in detail in order to learn more about the process of comet mass loss and meteoroid stream dynamics (Jenniskens et al. 1999).

NASA's 1998 Leonid Multi-Instrument Aircraft Campaign was designed to study the Leonid meteors with a wide range of imaging, spectroscopic and ranging techniques. Two aircraft were deployed to Okinawa, Japan, from where the Leond shower was observed during the night of November 17/18. To compliment the suite of instruments, I contributed a series of intensified video cameras that were intended to provide a record of meteors that were detected by other techniques. For example, the cameras would provide low resolution images of persistent trains, and images of meteors for correlation with debris trails detected by the University of Illinois Fe-lidar aboard one of the aircraft. The cameras also provided a record of the meteor flux for studies of the particle size distribution and meteoroid stream dynamics.

For the first time, a large enough number of cameras were deployed in a single experiment and under excellent observing conditions to provide sufficient numbers of meteors for a statistically significant detection of structures in the meteor shower activity curve from video records.

These flux measurements are complimented by records from several intensified video cameras at two widely separated sites in China at +1 and +2 time zones west from Okinawa, which provide flux information at times when twilight prevented further observations from Japan. For a map of the locations of these two double-station networks in the provinces of Hebei and Qinhai, see Jenniskens et al. (1999a).

METHODS

In anticipation of perhaps not so stellar meteor rates, I chose to deploy as many cameras as my budget allowed in order to detect sufficient meteors for analysis. Nine new cameras were developed that were flown on FISTA and Electra and one camera was added to three other intensified cameras deployed as part of the ground campaign , stationed at Xing Long (Hebei network).

I used a proven design consisting of low f-number optics, an AEG Multi Channel Plate XX1332 2nd generation image intensifier, and a Sony CCD-TRV65 Handycam Vision Hi-8 Camcorder that was optically coupled to the intensifier tube (Fig. 1). Two such cameras had been developed earlier and were used before for the purpose of multi-station The XX1332 image intensifiers have a large 48mm photocathode for high spatial resolution and a broad spectral range centered at the visual magnitude filter used to characterize visual magnitudes of background field stars (Fig. 2a). The response of the cameras is also determined by the transmittance of the aircraft windows, 3/4 inch optical quality BK7 glass on Electra and 3/4 inch optical quality what may be float glass on FISTA (Fig. 2b). However, it is the transmission of the f1.4/50mm objective lenses used on the intensified cameras (listed in Table 1) that determines the short wavelength cut-off.

The intensified camera is optically coupled to a Hi-8 Camcorder, which imprints a time stamp (per 1 second) in the video frames. The camcorder is mounted only 1 inch from the intensifier photocathode with almost no image distortion. The camera and intensifier were operated either from battery (300 mm system on FISTA and both cameras on Electra) or from the aircraft 110V power supply (all other systems). The 8mm tapes were changed every two hours.

Excerpts of video records can be found at: http://leonid.arc.nasa.gov/. The impression of meteors on the video camera is much the same as seen by a visual observer. The

resolution of 4.6' per line for the camera (with 50mm focal length optics) compares to about 3' resolution for the dark adapted naked eye. Moreover, daytime visual observers tend to be sensitive between about 4200 and 7000 Å, sometimes out to 3200-8350 Å, with a peak sensitivity at 5600 Å, although in night time conditions, different sensors in the retina become important and the peak sensitivity shifs somewhat towards the ultraviolet (e.g. Sidgwick 1980).

Cameras equipped with low f-number optics are most efficient in detecting meteors. 50 mm optics combines the benefits of a relatively slow motion across the sensor with a relatively small field of view that prevents too much mixing in of empty sky per pixel. Six 50mm cameras were deployed, four on FISTA and two on Electra (Table 1). Fig. 3 shows the position of the camera fields in polar coordinates. In each aircraft, two cameras were pointed at about 35 degrees altitude, while one additional set of two cameras on FISTA was pointed at 12 degrees altitude, thus covering most of the sky accessible from one side of the aircraft. Only a small fraction of the whole sky was covered. Adjacent cameras do not overlap. The camera nomenclature in Table 1 and throughout the paper successively lists aircraft, altitude, focal length and forward or back viewing direction (e.g. FH50R for FISTA, High, 50mm, Rearward).

There is a slight overlap with the high and low cameras on FISTA, but small enough to cause negligible error if treated as independent areas. Below 5 degrees altitude are the irregular tops of the cloud cover below the aircraft, which affects the rates in an unknown manner. Here, we will only consider meteors observed above 5 degrees altitude (that is, excluding the lower quarter of field of view from the low cameras).

Automatic software exists that can find meteors on video. I installed one such software package, MetRec by Sirko Molau of the International Meteor Organisation, and found that the detection rate was very sensitive to the settings of a number of parameters. Repeated visual inspection always resulted in higher numbers of meteors detected, unless the parameters for a small segment of tape were tuned just right. A demonstration of a second program by Pete Gural of SAIC showed a similar performance. High detection

rates are important to arrive at small statistical errors per unit time interval. Hence, I decided to visually inspect all the 50 hours of tapes that were recorded on Nov. 17/18.

Visual scanning demands extra attention in keeping the detection rate constant. The first inspection typically results in as low as 70±30% of meteors found, with significant variation in efficiency due to the level of concentration at any given moment (Fig. 4). Typically, lapses of concentration do not last long. A second inspection results in better than 90% of meteors detected, with a final less than 5% variation in detection efficiency from one time interval to the next. Averaging of rates from all cameras will average out such statistical variations. Amateur observers of the California Meteor Society provided support with the first tape inspection, while members of the Dutch Meteor Society examined the tapes from Delingha, Ulan, and Lin Ting Kou (Table 1).
imaging and flux measurements (Jenniskens et al. 1998). Only those meteors are counted that had their end point in the field of view. This avoids over counting early in the night when the trajectories are longer and a meteor is more likely captured in the field of view. The height of the end point is somewhat magnitude dependent and varies between 100 km for meteors of magnitude +6 to 85 km for meteors of magnitude -5 (Jenniskens et al. 1999). If the effect is ignored in influx calculations, rates of +6 meteors are overestimated by only 15% compared to -5 meteors. This is a negligible effect in the magnitude distribution, because the frequency of +6 and -5 meteors differs by a factor of 1000.

The aircraft traveled a pentagon shaped pattern during the mission, turning about every 20 minutes in a different direction (Jenniskens et al. 1999a). We considered only the periods of time when the camera was stationary with respect to the stars. The changing viewing direction also changes the viewing geometry with respect to the radiant. In order to improve the quality of the shower/non-shower classification, I initially plotted all meteors on gnomonic starcharts of the Brno Gnomonic Atlas (Lm = 6.5). All meteors of cameras E50F, E50R, FL50F and FH50R were thus plotted. I noticed considerable sporadic activity of fast meteors from eastern directions that, when wrongly classified, can affect the rate at early times in the night when apparent Leonid rates are still low. Later in the night, the high number of leonids makes classification by comparison

possible. Meteors of the final two cameras analyzed, FL50R and FH50F, were thus classified while watching the tapes, with no systematic differences in the flux curves compared to the similar cameras FL50F and FH50R.

Meteor magnitudes were derived by optical comparison with stars in the field of view. The stellar (V) magnitudes were derived from the Brno Gnomonic Atlas maps. The typical accuracy of magnitude estimates in such visual observations is of the order of ±0.7 magnitudes. Typically, the peak brightness of the meteor is considered. Leonids of apparent magnitude +3 and brighter (at 35 degrees altitude) tend to leave a recognizable wake. The faintest Leonids detected on the 50 mm cameras are of apparent magnitude +6.5, about 1 magnitude fainter than the star limiting magnitude (+7.5), as in visual observations.

In order to correctly estimate the flux of meteors brighter than magnitude 0, we used an additional camera with a wide angle lens (20 mm) that was aimed at the same area covered by each set of two 50 mm cameras on FISTA. Meteors that are too bright saturate the image in a manner that defeats direct comparison to background stars. Each camera has an 8-bit dynamic range, which limits the range of reliable magnitude estimates to about 5 magnitude. The wide angle optics was to dilute the meteor signal per pixel in order to make a different magnitude range accessible in an efficient manner. The limiting magnitude of these cameras was about 4 magnitudes less than the 50mm cameras. In addition, a Cokin Diffractor Universe special effect filter was mounted in front of these cameras, which decreased the limiting magnitude slightly, but which produced a striking low efficiency dispersion pattern in an ever changing pattern for each magnitude (Fig. 5). Absolute calibration was achieved by noting how each camera responded to the image of AO type star Sirius (V = -1.5), and the planet Jupter (V = -2.5).

For example, the brightest meteor detected by our cameras (Fig. 6) appeared about 11 degrees above the horizion at 18:06:18 UT and was measured to be of apparent magnitude +9 (absolute magnitude at 100 km distance of +11). A persistent train was imaged for a period of 22 minutes.

In order to extend the magnitude range to fainter magnitudes, we deployed one camera with a Tamron f2.8/300mm lens (shown in Fig. 1), which was aimed close to the zenith to detect intrinsically faint meteors. This camera detected Leonid meteors of apparent magnitude +9. However, the resulting spatial scale has a factor of 6 higher resolution than that of the 50 mm cameras. As a result, the angular velocity of the meteors across the pixels is higher by a factor of 6, leading to an expected loss of 2 magnitudes (Clifton 1971). Thus, the limiting magnitude was raised by a single magnitude to +7.

RESULTS

Visual observations

The November 1998 Leonid shower was the most impressive meteor event since the storm of 1966. Considerable excitement was created by the return of a broad two-day long component rich in bright meteors (Fig. 7). A similar component was seen in all years since 1994 (Jenniskens et al. 1996), but the 1995 return was particularly intense with abundant fireballs. An impressive all-sky image of the one European Network station with clear weather, containing 146 meteors brighter than -2 in a 4 hour exposure, testified to the magnitude of the spectacle. However, initial reports of up to 2000 meteors per hour seen from the Canary Islands turned out to be the result of group counts and, unfortunately, led to the misperception that the expected storm had peaked earlier than predicted.

The first reliable information on meteor flux was provided by visual observers around the globe. They were gathered and processed relatively shortly after the campaign by the International Meteor Organisation. Arlt (1998) found that observers in Europe did count only up to Zenith Hourly Rate (ZHR) = 400 meteors per hour at the peak of this bright component (Fig. 7). The Zenith Hourly Rate refers to the hourly count of a naked eye observer, after correction for radiant altitude dillution (1/sin (hr)), a personal perception, and for sky conditions as judged from the star limiting magnitude (Jenniskens 1994). A

secondary peak in the ZHR profile was detected on Nov. 17/18 when meteor magnitudes were on average somewhat fainter.

Our ZHR values calculated from counts by visual observers of the Dutch Meteor Society at the ground locations in China confirm the relative equal activity of Nov. 16/17 and 17/18 from locations in eastern Asia, with rates still somewhat elevated in the night of Nov. 18/19 (Betlem & van Mil 1999). However, Nov. 16/17 in particular was dominated by bright meteors, while Nov. 17/18 saw relatively more faint meteors. Our rates for Nov. 16/17 are a little higher than those calculated by Arlt, and we do not agree on details at the secondary maximum (Fig. 8). To my surprise, the activity of the annual shower may have been some 60% higher than in prior years (Jenniskens 1996), judging from rates prior to solar longitude $\lambda o = 233.7$ (Fig. 7). Some part of this may be due to classification errors whereby sporadic meteors are counted as Leonids.

Video data

Aboard Leonid MAC near Okinawa, Japan, we were particularly well located to observe any activity variations around the node of the comet orbit, which was at $\lambda o = 235.258^{o}$ (Epoch March 8.0 TT 1998). The time of the predicted maximum was uncertain. Estimates ranged from somewhat before the time of passing the comet node (e.g. the $\lambda o = 235.20$ by Brown & Jones 1993) to some time after passing the comet node (e.g. the $\lambda o = 235.338$ Jenniskens 1996). I hoped that some guidance to the peak time would come from the 1997 observations of the Leonids, but no secondary maximum was observed that year. Langbroek (1999) reported a possible secondary maximum in the 1996 Leonid data, as early as $\lambda o = 235.172$. Okinawa was chosen as a location to cover all these potential maxima. If the peak would be relatively late, the observations from China would cover the declining part of the curve.

Let us first examine the video records from ground-based observations in China. 1031 meteors from three nights are available for analysis. "ZHR" is now the hourly rate of Leonid meteors in 10-minute intervals, corrected for the geometric dilution caused by the radiant altitude (hr):

$$\text{"ZHR"} = N / (Teff \quad (\sin (h_r)) \qquad (1)$$

No effort is made to take into account the detection limit or spectral response of the instrument, or any other factor that would merely scale the counts. Of interest is the broad peak of meteors at around $\lambda o = 235.3$, present in the records of both networks in eastern and middle China (shown separately in Fig. 7). Each curve contains the counts of two camera systems. In the Hebei network, both cameras are independent. In the Qinhai network, both cameras monitor the same part of sky for multi-station work. The accuracy of the result is limited by the number of meteors in each time interval. This number is particularly low in the beginning of the night, when the radiant dilution is most severe. The errorbars are directly proportional to the root of the number of meteors in each interval:

$$\sigma \text{ "ZHR"} = \text{"ZHR"} / \bullet N \qquad (2)$$

Poisson statistics results frequently in significant deviations from the mean.

In comparison to these ground based observations, the flux measurements from the aircraft proved particularly effective. With similar cameras, two to three times higher rates were recorded by the "high" cameras, while the low cameras even picked up 4-6 times higher numbers of Leonids (Table 1). A total of 3200 meteors from the night of Nov. 17/18 are available for analysis. The low extinction at altitude paid off, especially near the horizon where the effective surface area covered is large. This came as a real surprise, because predictions made for clear sky ground-based observations predicted rates to decrease towards the horizon (Jenniskens et al. 1998, fig. 6). The calculations did not take into account the slower angular velocity of the meteors near the horizon and the very low extinction coefficients at altitude.

Figure 10 shows the Leonid rates measured from the high cameras aboard Electra and FISTA. If we consider the individual cameras, we note that the Electra records are most precise, with the FH50R camera hampered by higher shot noise caused by a faulty diaphragm and the meteors of the FH50F camera are not plotted for classification. If we take this into account, we can conclude that all cameras were similarly effective in detecting meteors, independent of azimuthal direction and platform. Rates are best measured late in the night, when highest numbers of meteors are observed because of smallest radiant altitude dilution. We note, however, that all cameras record highest "ZHR" around $\lambda o = 235.3$, producing peak rates in the early morning even after correction for this dilution.

Fig. 11 shows the mean Leonid rate of all "high" and all "low" cameras. The latter include only meteors that ended above 5 degrees altitude. Counts are high enough now to consider 5-minute intervals. Again there is a broad peak around $\lambda o = 235.3$. One high count at $\lambda o = 235.2$ jumps out in a single 5-minute interval in both sets of cameras. In comparison, sporadic (= non shower) meteor rates are constant during the night. The jump is followed by a strong decline in rates at $\lambda o = 235.22$ (Fig. 11). This decline coincides with a viewing direction towards the Leonid radiant, where angular velocities of the meteors are small. For graphs of angular velocity over the sky see Jenniskens et al. (1999). For a given viewing altitude, the angular velocity changes most dramatically near the radiant position. Fig. 12 shows the angular velocity of the Leonid meteors calculated for the center of the field of view during the night for cameras aboard Electra. Note that conditions are fairly constant with the exception of two intervals at $\lambda o = 235.22$ and $\lambda o = 235.30$. The lower count is counter intuitive, because one might expect significant longer exposure per pixel for meteors that move slower. This is shown in the graphs in Jenniskens et al. (1999). However, as already noted in the pioneering work by Clifton (1973), the meteors close to the radiant are not well detected by a visual observer. Recognition of the meteor highly depends on motion. We expect this effect to be strong when the angular velocity is very small. Hence, rates at $\lambda o = 235.22$ are probably underestimated, while rates at $\lambda o = 235.30$ are close to their actual values. Most affected is camera EF in the interval from 18:08-18:31 UT, when other cameras are also pointed

close to the Leonid radiant. We applied a small correction for this time interval , a factor of 1.1 for each affected camera to derive Figure 13. Fig. 13 also shows the data from the ground campaign, now scaled to those from the aircraft. Note that the two last data points from the airborne campaign are affected by twilight.

Population index

The Zenith Hourly Rate does not necessarily reflect the influx curve if the magnitude population index r = N(m+1)/N(m) changes across the profile. If the population index is low, then the count is dominated by bright meteors. Calculation of cumulative influx down to a small particle size limit will result in relatively small corrections. On the other hand, if the population index is large, then many faint meteors are missed due to the sensitivity limit of the camera.

The magnitude distribution of all meteors that were carefully compared with background stars are combined in Fig. 14. The counts for the high cameras (circles in Fig. 14) were shifted in magnitude to account for the smaller apparent brightness due to distance. The absolute magnitude is defined as the magnitude of the meteor were it observed at 100 km distance. Extinction by Rayleigh scattering accounts for only a fraction of a magnitude (Jenniskens et al. 1998). The sum amounts to an average shift of +1.6 magnitude for the Electra cameras and +1.35 magnitude for the FISTA cameras. The result is plotted
The (relatively few) bright meteors with apparent magnitude < -1 were treated in a different manner. I determined the altitude of all bright meteors and derived an absolute magnitude for individual meteors. All meteors that appeared above 10^{o} altitude were selected. Hence, data are obtained for meteors of magnitude -3 and brighter. The data are scaled to the counts of the high cameras by the ratio of the effective surface areas covered.

Finally, the magnitude distribution of the F300 camera was taken as-is: all trails were counted, also those that left the field of view. This can be done without penalty because

the trail length does not change much anymore below magnitude +4 (Jenniskens et al. 1998). The rates are simply scaled to those of the high cameras by matching the count of the brightest meteors. Note that there is a significant loss of sensitivity below +4 magnitude for the high cameras due to non-homogeneous sensitivity limit across the images for faint meteors. The 300mm camera suggests that counts continue to increase exponentially with magnitude.

I find no significant variation of the population index over a wide magnitude range. From the bright meteor tail of a plot of the number of meteors versus magnitude, a mean value of $r = N(m+1)/N(m) = 1.8 \pm 0.1$ is found for our Leonids and $r = 2.7 \pm 0.2$ for the sporadic meteors. The latter value is thought to be $r = 3.4$ (Jenniskens 1994), and may be less because of bright Taurid meteors in the sample.

I also studied the variation of population index over the night of Nov. 17/18 (Fig. 15). The observed rate was corrected with a detection probability function P(m) that was derived from the deviation of the mean count N(m) in Fig. 14 from an exponential curve. For the high cameras, I find that nearly all of +4 Leonids, 60% of +5 and 19% of +6 Leonids. At the same time, 100% of +4 sporadics were found, 54% of +5 sporadics and 10% of +6 sporadics. The exponential fit assumed was slightly steeper than derived when including the bright meteor sample, i.e. $r = 1.9$ instead of $r = 1.8$, hence the mean of the values in Fig. 15 are slightly larger than 1.8.

The result is in good agreement with values by Arlt (1998), shown as open symbols. There is some variation of r that is symmetric around the position of the comet node at 235.258, but that can not be correlated with features in the flux profile of Fig. 13, with the exception of one spike with high numbers of faint meteors, which corresponds with the spike in meteors observed in the flux curve at $\lambda o = 235.195$. This spike is so brief in duration that it is likely caused by a single fragmented meteor.

We do not have sufficient meteors detected in the night of Nov. 16/17 (ground data only) to calculate an accurate population index. Arlt derived a population index of only $r = 1.3$

at the peak of this component. This is a very unusually low value for meteor showers. Typically, values are in the range of 2.5 to 3.2 (Jenniskens 1994). Our frequency of Leonid detections suggests a larger value of r, but not as large as on the night of Nov. 17/18. A value of r ~ 1.5 would bring the ZHR values of Fig. 7 down to the observed relative rates in the night Nov. 16/17 and 17/18.

The influx

The activity scale of Fig. 13 is directly proportional to influx. The conversion involves the effective observing area of each camera and the fraction of meteors missed due to sensitivity of the cameras below the limit (set at +6.5 magnitude).

I calibrated the counts on the flux measured with the high cameras, which had an effective area of 12000 and 8200 km^2 for Electra and FISTA cameras respectively, aligning the low cameras to the "ZHR" of the low cameras. Hence, the sensitivity and spectral response of the high cameras determines the cut off at +6.5 apparent magnitude, or about +5.0 absolute magnitude. I also correct for the fraction of missed faint meteors, determined from the observed magnitude size distribution (Fig. 14), which amounts to a factor of 3.
The result is shown in Fig. 16. The absolute values derived are in excellent agreement with estimates from visual observations by Arlt (1998) shown as a dashed line in fig. 16.

The step from Zenith Hourly Rate to influx consists of one other correction in the case of visual observers. The ZHR does not take into account that visual observers pick up bright meteors over a much larger surface area. If that correction is made, the prominent peak in Fig. 7 all but disappears. Arlt found the broad component to have negligible flux if meteors < 6.5 magnitude are considered (Fig. 17, solid line).

The video data do not need such correction. Hence, the video counts can be used to derive influx independent from the magnitude distribution index, as long as the limit is setat pr abpve the sensitivity limit of the instrument. The dashed line in Fig. 17 is drawn assuming that the broad background component has the same width as in prior years (i.e.

B = 1.1, Jenniskens 1996). The peak of the curve is set by the results of Arlt (1998) at λo = 234.52. The ascending slope is well observed from the ground-based video observations in China. This sets the peak flux at "ZHR" = 65±5 on the activity scale of Fig. 13.

We conclude that the broad component did contribute significantly to the influx of meteors of magnitude +6.5 and brighter. However, in comparing Fig. 7 and 17, we confirm that what others considered the "secondary maximum", or even a disappointing spectacle, was in fact the peak of the influx curve. We were at the right place at the right time for viewing the highest fluxes. Viewers in Europe saw per saldo more bright meteors, but not much more than other observers in the world fortunate enough to observe both nights of Nov. 16/17 and 17/18.

DISCUSSION

Recent models of the Leonid meteoroid stream (Asher 1998, 1999) have drawn attention to small scale structure in the meteoroid stream that represent individual ejecta deposited at the different returns of the comet. Each return, the orbit of the comet has changes slightly as a result of planetary perturbations and therefore the ejecta of large submm-cm sized grains are deposited in slightly different orbits. Over time, the dust continues to spread out along the comet orbit in a trail-like structure due to small orbital period variations from one dust grain to the next and planetary perturbations on individual orbits tend to disperse the trails gradually. Until recently, it was assumed that the ejecta of all epochs would be merged into one dust trail. Now, it is believed that individual returns can be recognized when Earth passes these relatively recent ejecta.

Our data provide the outline of a narrow dust component superposed on the background of the broad component and the annual stream background. The profile is much wider than during previous observations of Leonid storms, when the characteristic (2 x 1/e) width of $\Delta\lambda o$ = 0.029 degrees (Jenniskens 1995). This provile has a width of 0.14 degrees. The profile is characteristically non-Gaussian and non-Lorenzian. A good fit needs at least two symmetric components of the characteristic form:

$$"ZHR" = "ZHR_{max}" \ 10^{(B \mid \lambda o^{max} - \lambda o \mid)} \quad (3)$$

The fit shown in Fig. 16 has two components with B = 6±1 and λo = 235.280±0.005 with "ZHR_{max}" = 60 and B ~ 30 at λo = 235.320 with "ZHR_{max}" = 50. These values of B were chosen to be identical to those derived from profiles of past Leonid meteor storms (Jenniskens 1995, 1996). While in other years, the B=6 component provided a background to the main peak, this time the components were separated.

It is not clear if the narrow component responsible for the steep decline of rates can be equated to the dust trail responsible for recent meteor storms. We have no strong evidence for the narrow component having the r = 3.0 as in past meteor storms (Fig. 15).

Our observations are consistent with Earth meeting ejecta of different epochs, causing sussesive maxima. Note that this not mean that there is filamentary structure with large variations in maxima and minima. Rather, the flux curve is composed of a number of debris components that have blended. A direct comparison with theory may allow the identification of the epoch of ejection of the debris, but such work is outside the scope of this paper.

Acknowledgments - Many people contributed to the success of this experiment. The cameras were developed with financial support of NASA Ames Research Center's Directors Discretionary Fund. Gary Palmer of EM Engineering constructed the hardware and Mike Koop of Lockheed-Martin provided the electronic circuits. We thank FISTA and Electra operators who helped install the cameras. Special thanks goes to Norm Zrubrek of the NCAR Research Aviation Facility in Broomfield. Mik Koop operated the cameras onboard FISTA, with help of Steve Butow, while Mike Wilson assisted in the operation onboard Electra. NASA's Leonid MAC was supported by NASA Ames Research Center and by NASA's Planetary Astronomy Program, Exobiology Program and the Astrobiology Advanced Missions and Technology program. We thank Hans Betlem and Olga van Mil who provided a summary of visual observations. Jane Houston,

Mojo, Mark Taylor and Ben … of the California Meteor Society (CMS) and David Nugent helped scan the video tapes. The video cameras at the ground site in China were owned and operated by Carl Johannink and Casper ter Kuile (Ulan) Romke Schievink (Delingha) and Klaas Jobse (Lin Ting Kou). CMS member Ming Li operated the Xing Long camera and helped coordinate the effort. Financial support for the ground-based campaign was provided by the Dutch and Chinese Academies of Sciences, the Leids Kerkhoven-Bosscha Fonds and the NASA Planetary Astronomy program.

Editorial handling:

REFERENCES

Arlt R. (1998) Bulletin 13 of the International Leonid Watch: the 1998 Leonid Meteor Shower. WGN, the Journal of the IMO **26**, 239-248.

Asher D.J., Bailey M.E., Emel'yanenko V.V. (1999) Resonant meteoroids from Comet Tempel-Tuttle in 1333: the cause of the unexpected Leonid outburst in 1998. *Mon. Not. R. Astron. Soc.* **304**, L53-L56.

Asher D.J. (1998) The Leonid meteor storms of 1833 and 1966. *Mon. Not. R. Astron. Soc.* XXX, XXX-XXX

Beech M., Brown P. (1994) Space platform impact probabilities - the threat from the Leonids, *ESA J.* **18**, 63-73.

Betlem H, Van Mil O. (1999) *Radiant* **21** (1999) pp. 65 ev.

Brown P., Jones J. (1993) Evolution of the Leonid meteor stream. In Meteoroids and their parent bodies. J. Stohl, I.P. Williams (eds.), Astronomical Inst., Slovak Acad. Sci., Bratislava, 1993, pp. 57-60.

Brown P., Simek M., Jones J. (1997) Radar observations of the Leonids: 1964-1995. *Astron. Astrophys.* **322**, 687-695.

Brown P., Simek M., Jones J., Arlt R., Hocking W.K., Beech M., (1998) Observations of the 1996 Leonid meteor shower by radar, visual and video techniques. *Mon. Not. R. Astron. Soc.* **300,** 244-250.

Clifton K.S. (1971) Airborne meteor observations at high latitudes. NASA Technical

Note D-6303 , 49pp.

Clifton K.S. (1973) Television studies of faint meteors. *J. of Geophys. Res*. **78**, 6511-6521.

Hapgood M.A. (1980) IR observation of a persistent meteor train. *Nature* **286**, 582-583.

Jenniskens P. (1994) Meteor stream activity I. The annual streams. *Astron. Astrophys*. **287**, 990-1013.

Jenniskens P. (1995) Meteor stream activity II. Meteor outbursts. *Astron. Astrophys*. **295**, 206-235

Jenniskens P. (1996) Meteor stream activity III. Measurement of the first in a new series of Leonid outburst. *Meteoritics & Planetary Science* **31**, 177-184.

Jenniskens P. (1998) Preparing for the return of the storming Leonids. *Meteoritics & Plan. Sci.* **33**, 955-957.

Jenniskens P. (1999) Update on the Leonids. *Plan. Space Science* (in press)

Jenniskens P., Betlem H., de Lignie M., ter Kuile C., van Vliet M.C.A., van 't Leven J., Koop M., Morales E., Rice T. (1998) On the unusual activity of the Perseid meteor shower (1989-96) and the dust trail of comet 109P/Swift-Tuttle. *Mont. Not. R. Astron. Soc.* **301**, 941-954.

Jenniskens P., de Lignie M., Betlem H., Borovicka J., Laux C.O., Packan D., Kruger C.H. (1999) Preparing for the 1998/99 Leonid Storms, in*: Laboratory Astrophysics and Space Research*, P. Ehrenfreund et al. (eds.), Kluwer Academic Publishers, p. 425-455.

Jenniskens P. et al. (1999a) The 1998 Leonid Multi-Instrument Aircraft Campaign. Meteoritics & Planetary Science, this issue.

Langbroek M. (1999) Leonid outburst activity 1996: A broad structure and a first occurrence of a narrow peak of fainter meteors. *Meteoritics & Plan. Sci.* **34**, 137-145.

MacIntosh B.A., Millman P.M., (1970) The Leonids by radar - 1957 to 1968. *Meteoritics* **5**, 1-…

Sidgwick (1980) Amateur Astronomer Handbook.

Yeomans D.K., Yau K.K., Weissman P.R. (1996) The impending appearance of comet Tempel-Tuttle and the Leonid Meteors, *Icarus* **124**, 407-413.

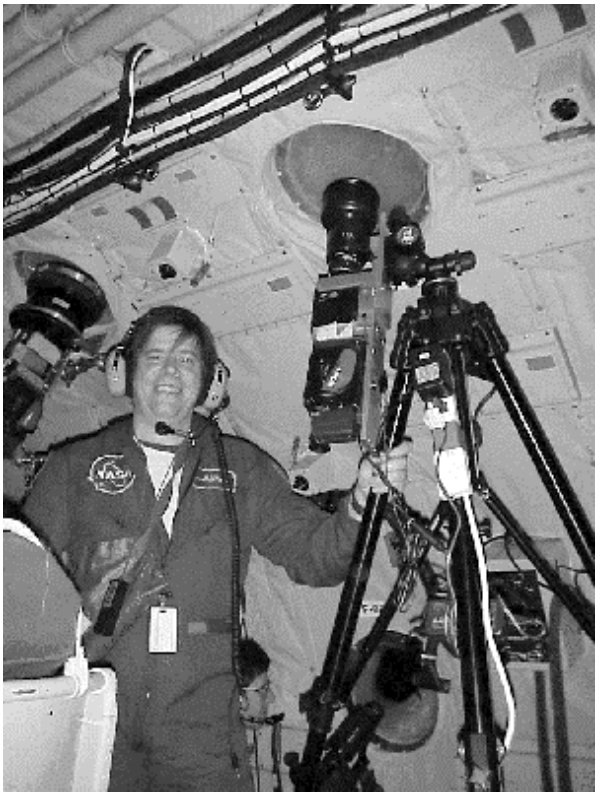

Fig. 1. Amateur astronomer Mike Koop operated the intensified video cameras onboard FISTA. Shown is camera F300.

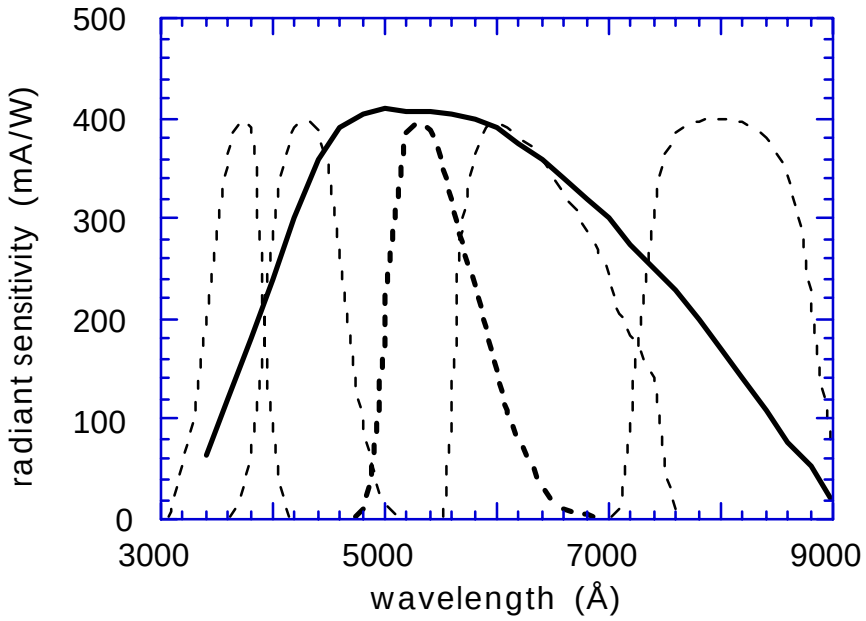

Fig. 2a. Radiant sensitivity of the photocathode Type S25 of the XX1332 Intensifiers (factory specification). Superposed are the UB**V**RI photometric filters (from left to right) used to characterize stellar magnitudes.

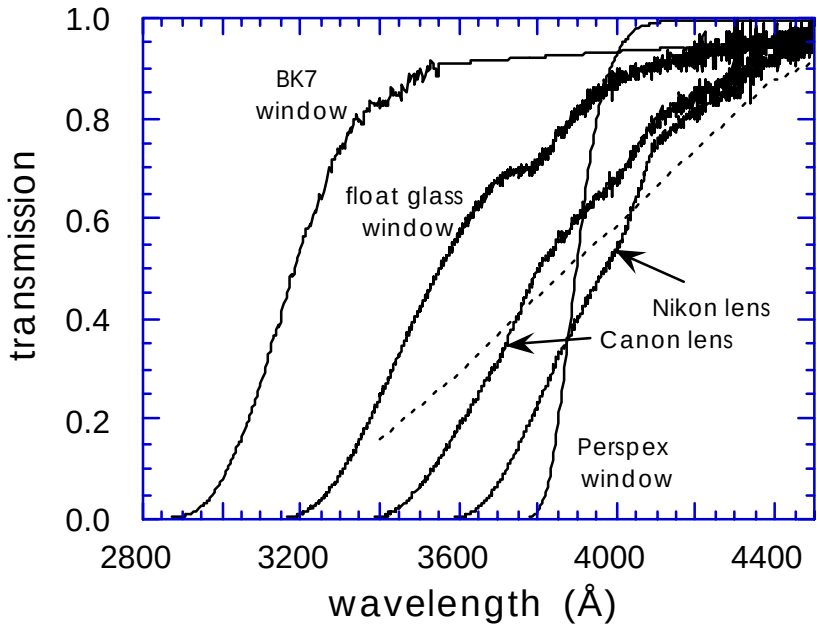

Fig. 2b. Measured spectral transmission curves compared to image intensifier photocathode radiant sensitivity.

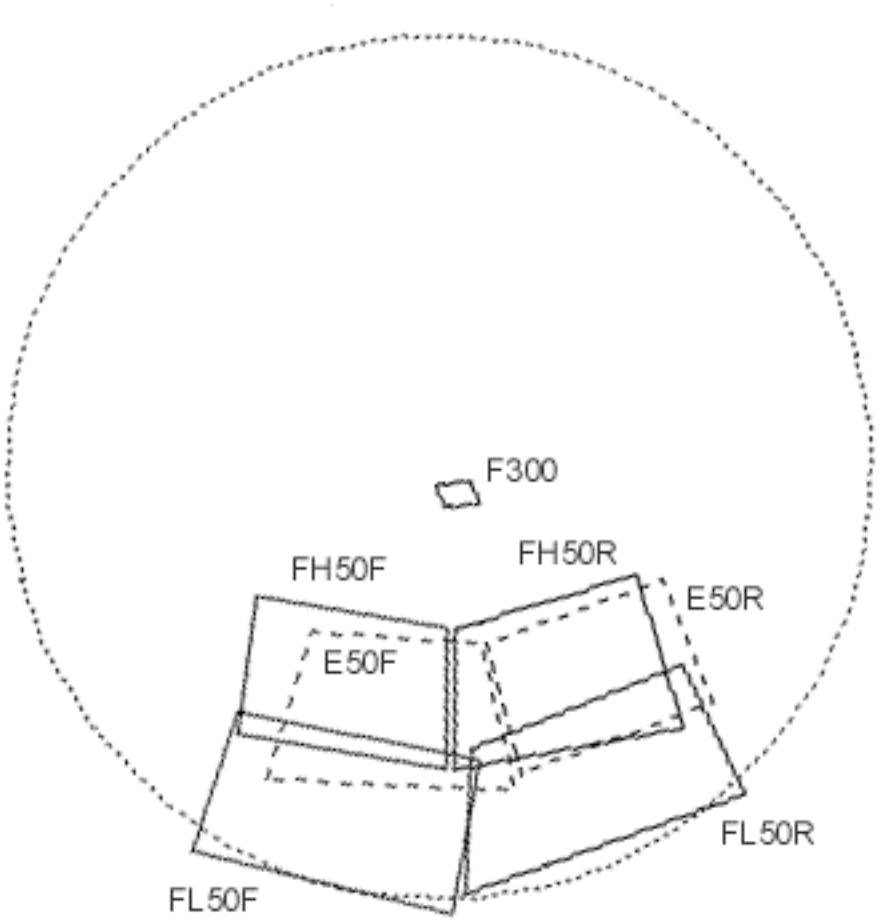

Fig. 3. Camera fields on FISTA (solid lines) and Electra (dashed lines) in altitude and azimuth polar coordinates. Dashed line is horizon.

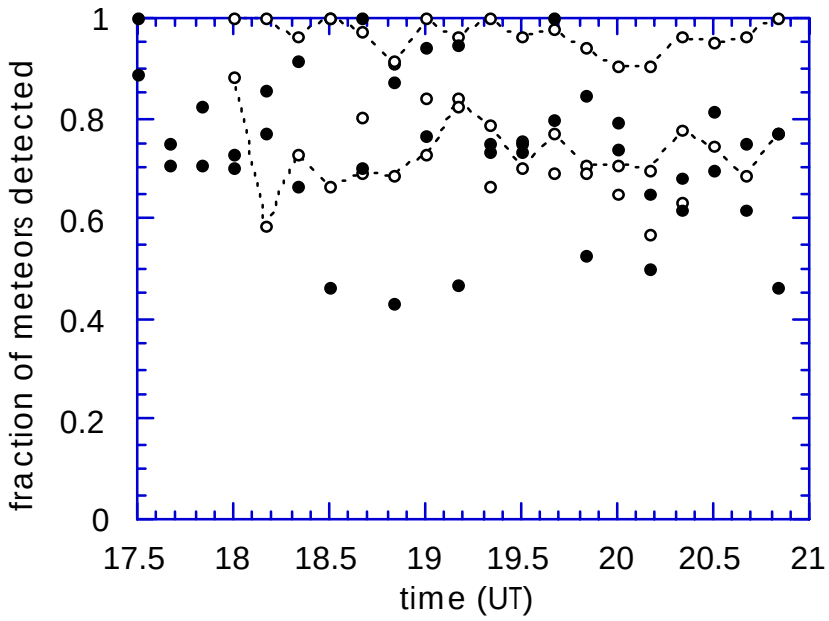

Fig. 4. The fraction of all meteors found during the first inspection of the tapes. Open circles show data for low cameras, solid circles are high camera fields. The dashed line are data for FL50F, including faint meteors that were not recovered in the second inspection (top curve), which were excluded from further analysis.

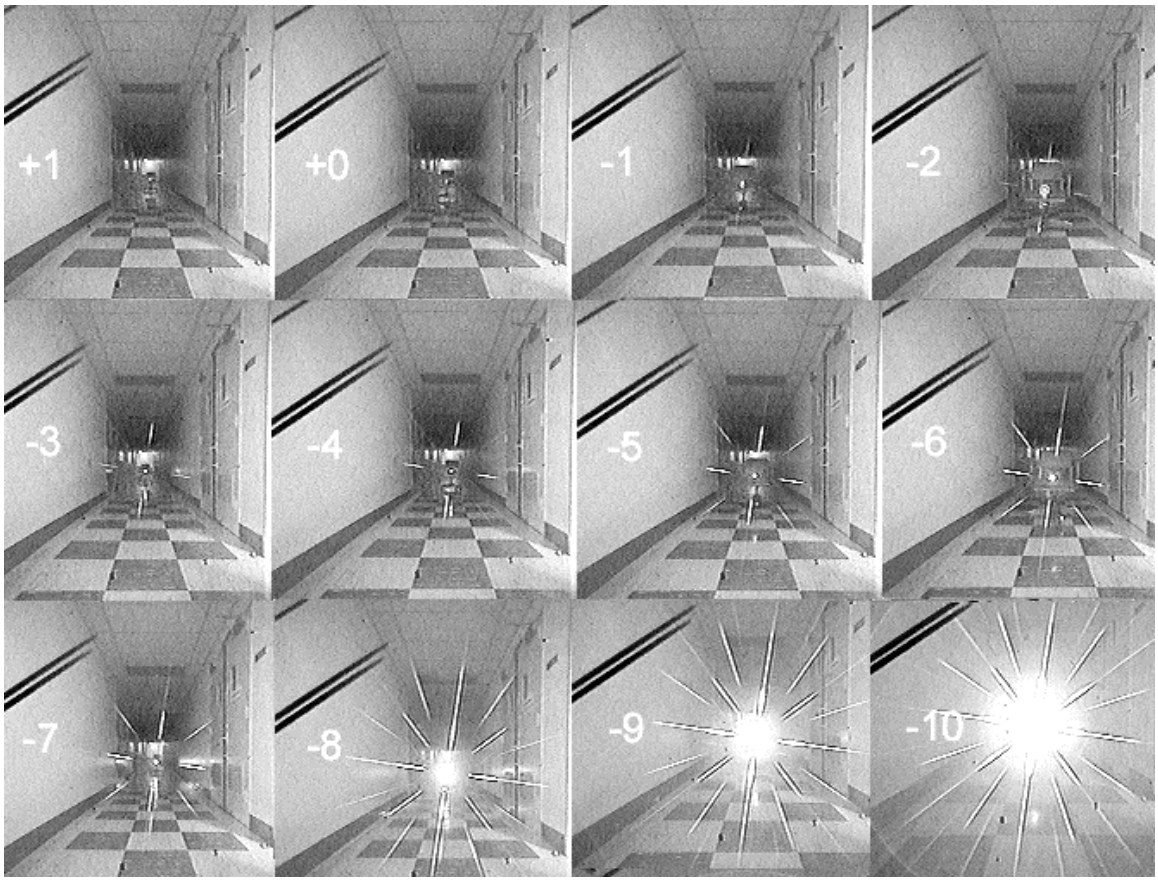

Fig. 5. Calibration of meteor magnitudes from pattern induced by low efficiency diffraction grating (FL20).

Fig. 6. The bright fireball of 18:06:18 UT as observed by the 50mm (top) and 20mm (bottom) cameras.

.

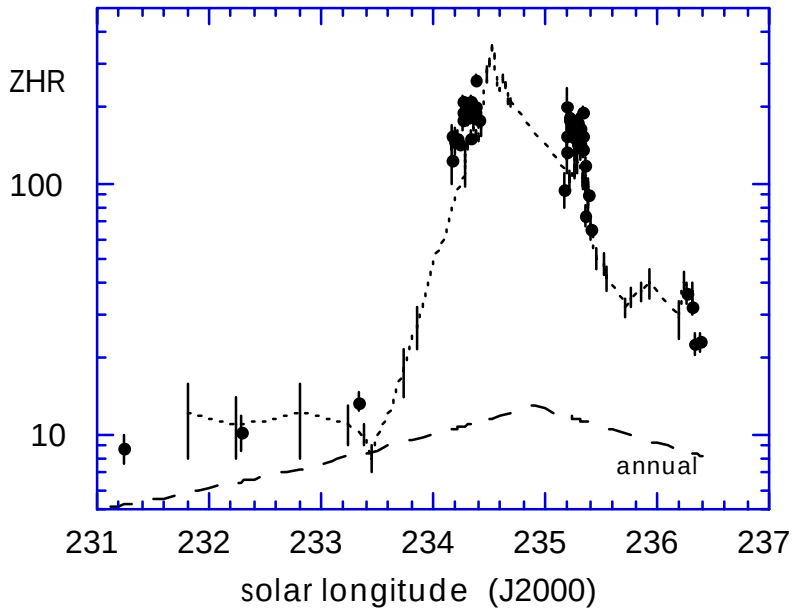

Fig. 7. Zenith Hourly Rates of the 1998 Leonid shower calculated from the meteor counts of visual observers in China (•). The dashed line shows results by Arlt (1998).

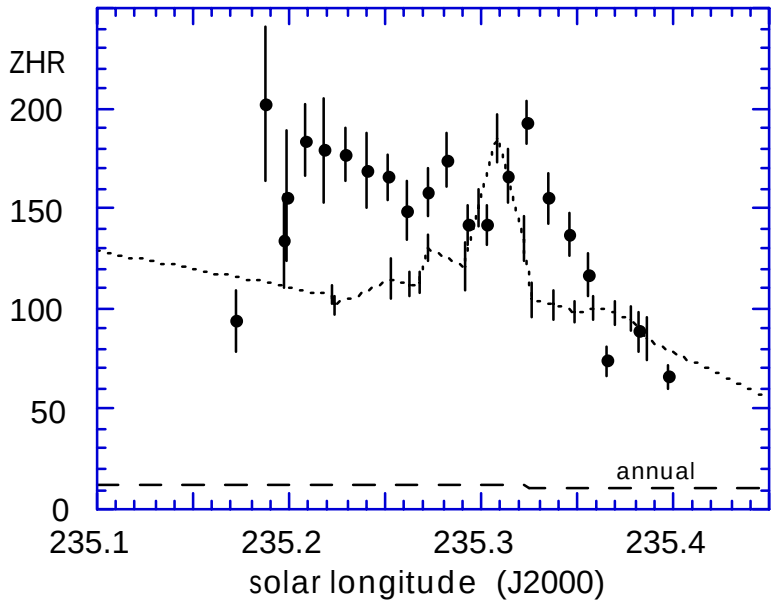

Fig. 8. Detail of Fig. 7 at the secondary peak in the night of Nov. 17/18.

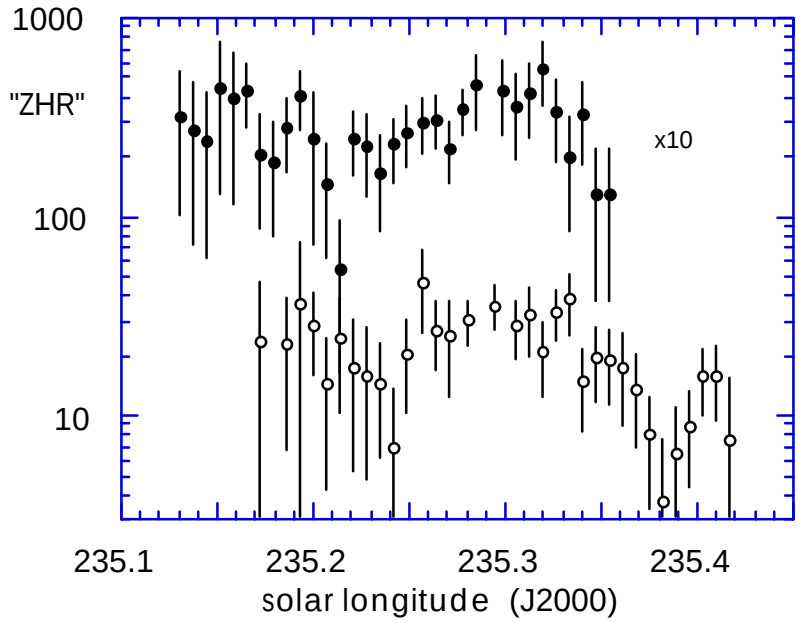

Fig. 9. Video flux rates from ground-based cameras in Xing Long and Lin Ting Kou of the Hebei network (solid points) and Delingha and Ulan of the Qinhai network (open points) in 10 minute intervals.

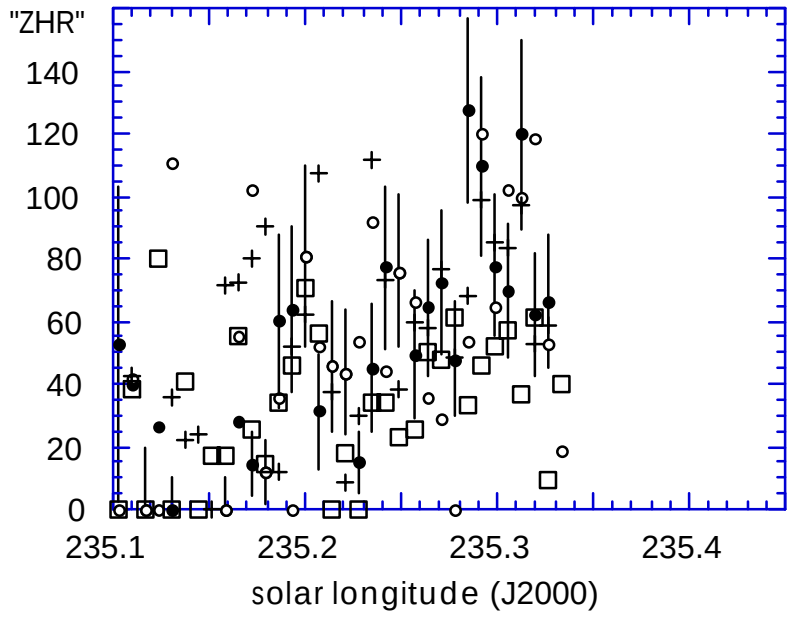

Fig. 10. Counts of individual "high" cameras. Symbols: • = E50F, o = E50R, square = FH50R, + = FH50F.

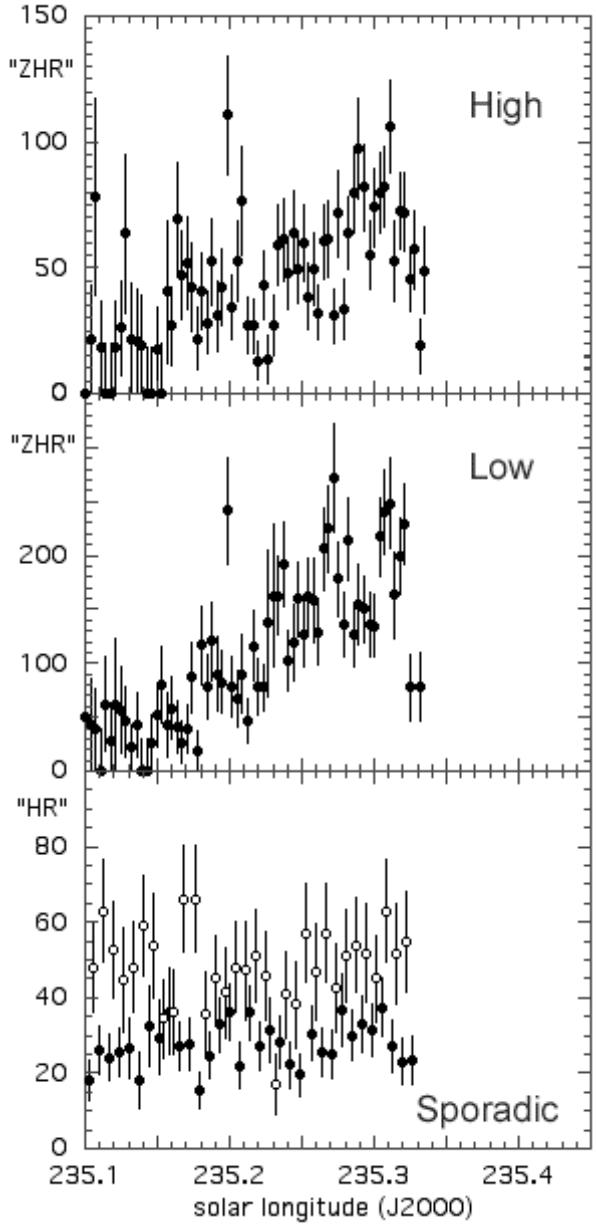

Fig. 11. 5-minute counts corrected for radiant dilution. Top graph: high altitude data, middle graph: low altitude cameras. Bottom graph shows mean sporadic rates for high (•) and low (o) cameras (10 minute counts - low cameras displaced in solar longitude for clarity).

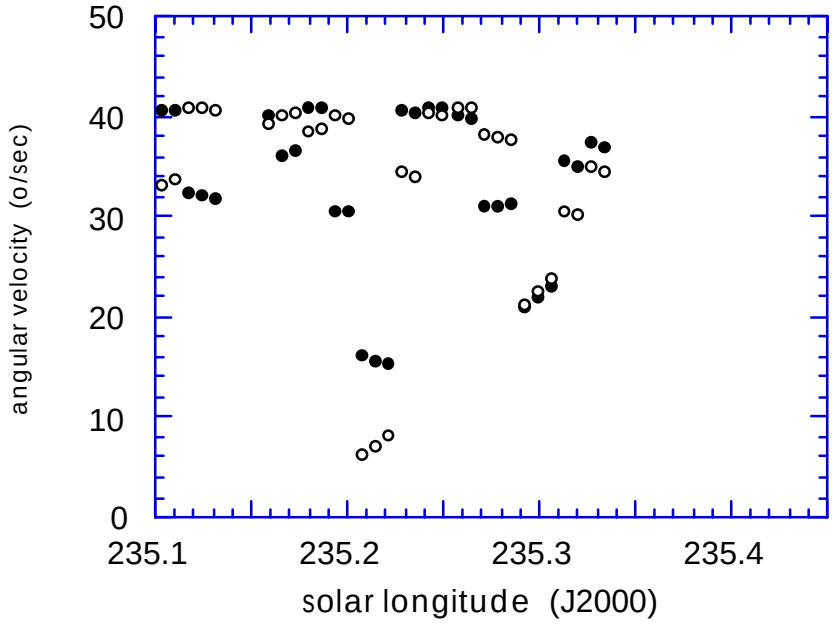

Fig. 12. Angular velocity of meteors in the center of the field of view from the Electra Rearward (•) and Forward (o) cameras.

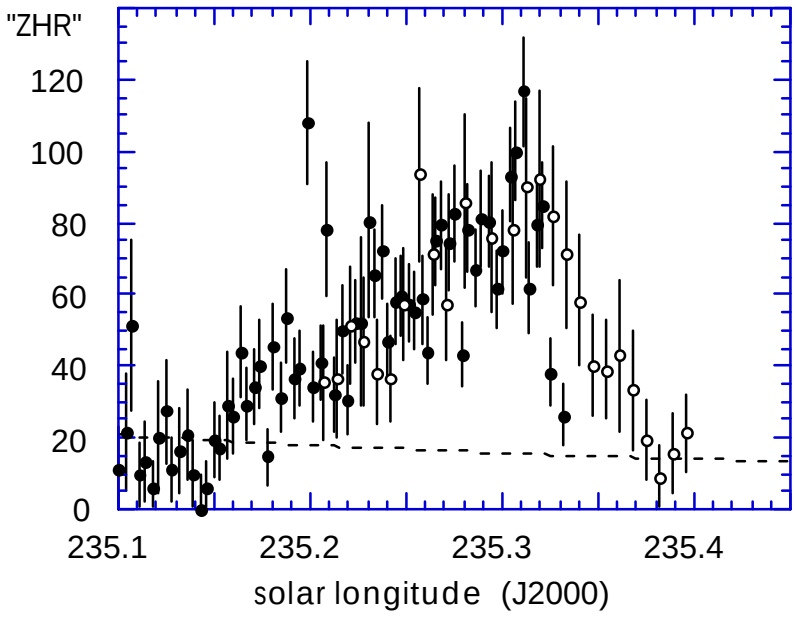

Fig. 13. Mean rates from the aircraft and from the ground (scaled to those of the aircraft).

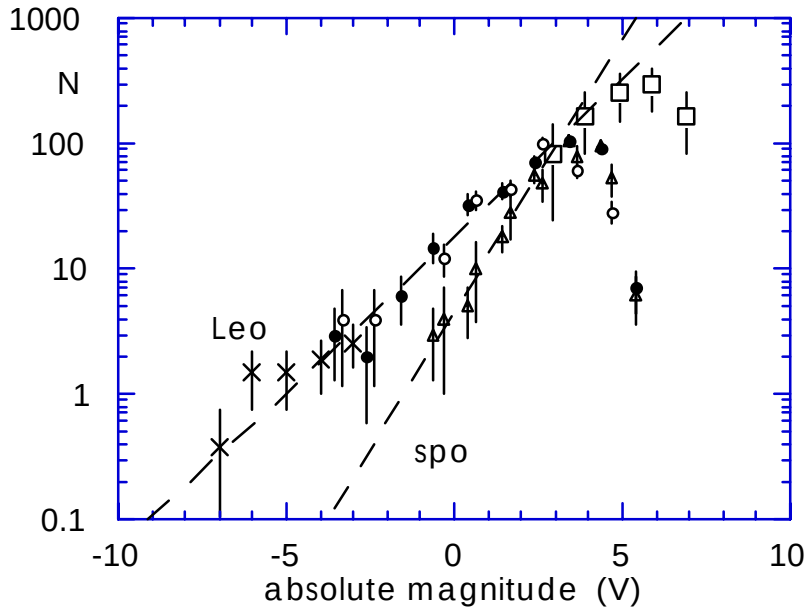

Fig. 14. Magnitude distributions of Leonid and non-Leonid (sporadic) meteors.

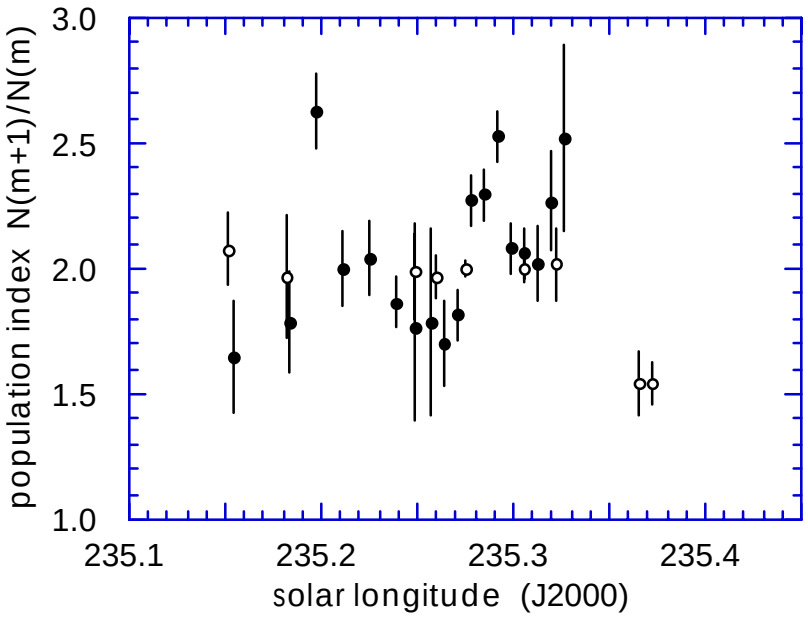

Fig. 15. Population index N(m+1)/N(m). Black dots: video data. Open circles: Arlt (1998).

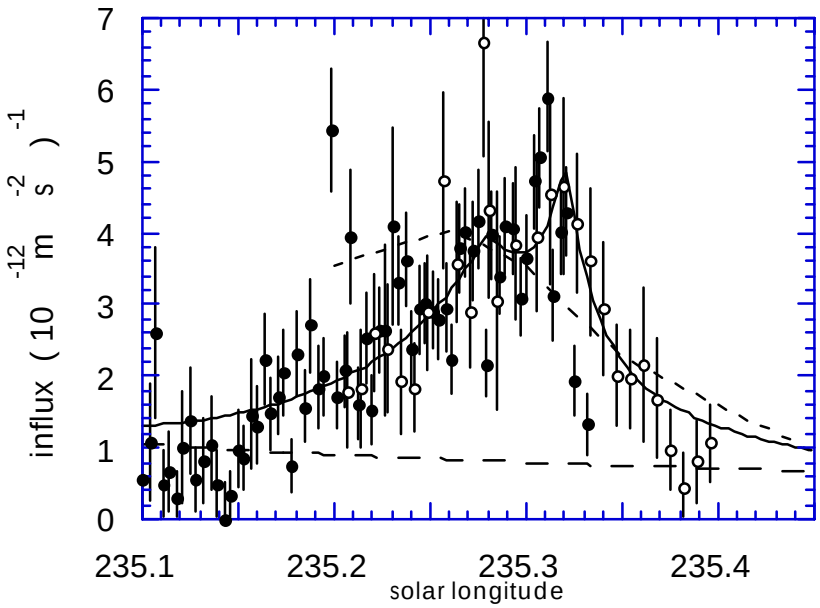

Fig. 16. Meteoroid influx for particles smaller than those producing absolute magnitude +5.0 magnitude meteors (masses less than about 7 x 10^{-5} g).

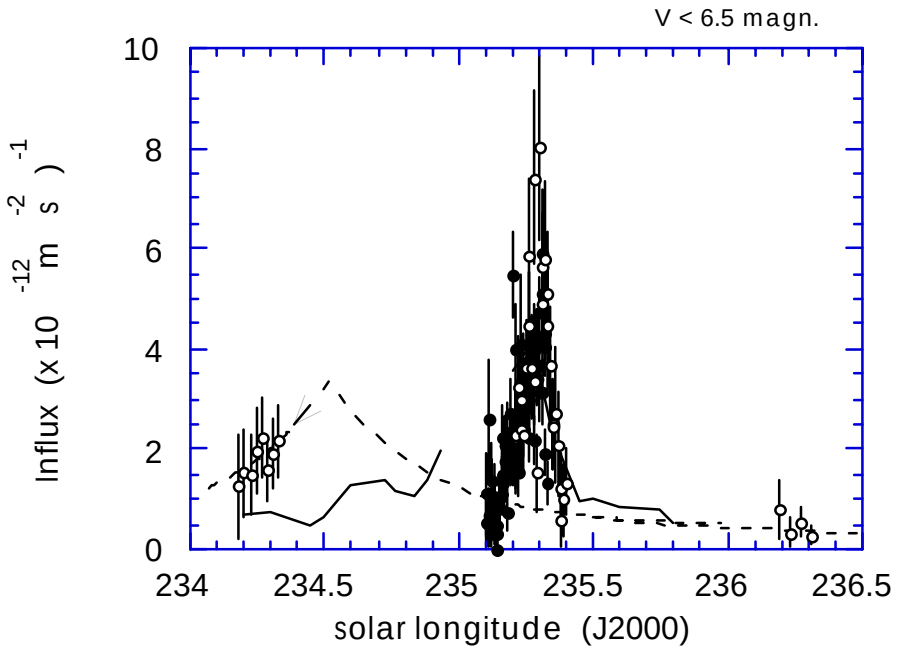

Fig. 17. As fig. 16.

Table 1. Intensified cameras.

	Cameras:	Intensifier:	Altitude: o)	o)	star Lm: magn.	Ntot:	Teff: (h)	ZHR/<ZHR>
Electra:								
E50F	Canon 50mm f1.4	XX1332	32	39x29	+7.5	360	4.6	0.9
E50R	Canon 50mm f1.4	1332	33	39x29	+7.5	245	4.6	0.8
FISTA:								
F300	Tamron SP 300mm f2.8	1332	82	7x5	+10.0	110	5.7	-.-
FH55F	Nikon SC 55mm f1.2	1332	36	35x26	+7.5	350	5.5	0.9
FH50R	Nikon 50mm f1.4	1332	36	39x29	+7	330	5.9	0.44**
FL50F	Canon FD 50mm f1.4	1332	12	39x29	+7.5	1010	5.8	2.2
FL50R	Canon 50mm f1.4	1332	12	39x29	+7.5	790	5.8	1.7
FH20	Nikon AF 20mm f2.8D*	1332	36	85x60	+3	20+	5.8	-.-
FL20	Nikon AF 20mm f2.8D*	1332	12	85x60	+3	20+	5.8	-.-
China - Hebei network:								
Xing Long	Canon FD 100mm f2.8	1332	22	27x19	+8.1	130	2.7	0.32
Lin Ting Kou	Canon 50mm f1.2	1332	50	38x30	+7	391	10.3	0.54
China - Qinhai network:								
Delingha	Sony 25mm f1.8 Delnocta-TS		57	28 circl.	+7.0	277	15.5	0.37
Ulan	Canon FD 1.2/55mm SSC	1400	57	28 circl.	+8.5	233	5.8	0.38

*) with Cokin Diffractor Universe special effect filter
**) higher level of shot noise